Tunning the Crystallization Behavior of B2O3 – SiO2 – Bi2O3 – TiO2 – Y2O3 Glasses

kh. S. Shaaban (khamies1078@yahoo.com)
Al-Azhar University https://orcid.org/0000-0002-5969-3089

Research Article

Keywords: Glasses, Y2O3, FT-IR, DTA, XRD, SEM

Posted Date: March 23rd, 2021

DOI: https://doi.org/10.21203/rs.3.rs-346000/v1

Tunning the crystallization behavior of $B_2O_3 – SiO_2 – Bi_2O_3 – TiO_2 – Y_2O_3$ glasses

Kh. S. Shaaban[1,*]

[1]Chemistry Department, Faculty of Science, Al-Azhar University, P.O. 71524, Assiut, Egypt.

ABSTRACT

Glasses with the chemical composition of $52B_2O_3 – 12SiO_2$- $26Bi_2O_3 – (10 - x)TiO_2$ - xY_2O_3, : $(0 \leq x \geq 10)$ prepared using the melt-quench method. The goal of this study is to investigate the structural, thermal, and crystallization characteristics of these samples. XRD analysis has explored the nature of the glass system. Molar volume obtained reduced while the density denotes increased in the present system. FTIR analysis revealed that as Y_2O_3 replaced by TiO_2, because of an increasing trend in bridging oxygens (BOs), structural units and interconnection of modifier oxide tetrahedral increment, while non-bridging oxygens (NBOs) reduce. These glasses' thermal stability investigated using DTA. As the concentration of Y_2O_3 increased, so the thermal parameter values. The glass-ceramic denoted prepared under controlled heat and investigated using XRD & SEM. Ultrasonic velocities and elastic moduli of glass-ceramic samples increase as internal energy increases. The significance of Y_2O_3 modifier in the glass system signifies proved. Y_2O_3 is a powerful nucleating agent that can cause crystallization, assisting in the formation of glass-ceramic phases.

Keywords: Glasses; Y_2O_3**;** FT-IR, DTA; XRD, SEM

***Corresponding Authors: Emails:** khamies1078@yahoo.com,

1. Introduction

Due to the importance of glass materials containing many transition metal ions (TMI) for many applications, these glasses have existed intersected over the past few years. In specific, the glass based on B_2O_3 and SiO_2 has become common among a wide variety of glass systems, keeping in mind its glass status, transparency, and a variety of physical and chemical properties. The B element can transform its coordination number between 3 and 4 with oxygen supplying by modification of metal cations [1-5]. Due to their unique properties such as hardness, transparency, UV-transmission ability, and corrosion resistance, SiO_2-B_2O_3 glasses investigated for many years. B_2O_3- SiO_2 glass modified with Bi_2O_3 characterized by its excellent optical, mechanical, radiation, and electrical properties [5-12].

The physical characteristics of the glass change based on its formulation and can linked with the network structures and interatomic forces. Glasses with higher levels of bridging oxygen (BOs) have a more compact glass framework and high elastic moduli. Introducing Y_2O_3 to SiO_2 - B_2O_3 glasses provide chemical stability durability, a vast compositional variety of glass forming, and increased transmission with promising properties reported. The presence of trivalent oxide like Y_2O_3 in borosilicate glass exhibits dual nature as former or intermediate in the glass network. These glasses obtained noticed to withstand atmospheric moisture and are accept a good quantity of doping transition metal (TM) or rare-earth (REs) [13-14].

Glasses doped intermediate oxides such as TiO_2 and Y_2O_3 have specific mechanical and optical characteristics such as hardness, elastic moduli, and higher refractive index [15-18]. It is also significant to observe that the inclusion of Y_2O_3 improves the capability of UV transmission, enhances thermal stability and chemical durability. The emergence of Y_2O_3 into the glass network improved the glass's mechanical, thermal, and crystallization characteristics. Because of their excellent conductivity, these samples in ionic terms, it is probable to use them in UV optics, solid-state batteries, and radiation protection. These glasses have a higher

refractive index and less photon energy than other glasses. The significant development of B_2O_3 – SiO_2 – Bi_2O_3 – TiO_2 – Y_2O_3 glasses are extremely important in both science and technology. The creativity of this research paper reflected in the structural, thermal, and crystallization characteristics of B_2O_3 – SiO_2 – Bi_2O_3-TiO_2 glass undoped and doped with Y^{+3} ions.

2. Methodology

Five glass samples in Table 1 with the nominal compositions $52B_2O_3$ – $12SiO_2$ – 26Bi2O3- TiO_2- Y_2O_3, prepared using the solid-state conventional method. By melting together specific weights of B_2O_3 in the form of H_3BO_4 (Merck), SiO_2 (Aldrich), Bi_2O_3 (Merck), TiO_2 (Merck), and Y_2O_3 (Merck) in an open porcelain crucible. H_3BO_4 converted into B_2O_3 after the H2O evaporation process throughout the melting in porcelain crucibles. Thus, it is possible to estimate the required amount of oxide to match the chemical formula used by knowing the molecular weight of H_3BO_4, and B_2O_3. The porcelain crucible with the blend kept at 650 °C for 45 minutes to decrease the tendency to volatilize. The furnace temperature programmed to rise to the melting temperature at 1150 °C and kept for 50 minutes. The melting glass was cast in a clean stainless-steel mold. After that, glass samples annealed at 400 °C to remove the internal stresses.

To verify the status of fabricated glasses, and glass-ceramics the Philips X-ray diffractometer (model PW/1710) used. Using the KBr pellet technique, an infrared spectrophotometer of type JASCO, FT/IR-430 (Japan), quantified the FT-IR spectrum of these samples in the wavenumber region of 400 - 4000 cm^{-1} at ambient temperature. To allow us to shed further light on the modifications of the various structural units, the resulting spectrum deconvoluted. DTA-50 For thermal investigation, (Shimadzu- Japan) was used. The glass-ceramics have obtained by heating the glasses in an electrical furnace at 650 C for 2 h and at 780 C for 1h at a heating rate of 40 C/m, then cooling to room temperature.

The surface morphology of some bulk glass-ceramic samples is studied using a scanning electron microscope, by electron microscope model A Jeol (JSM-T20, Tokyo, Japan). The densities of glasses and glass-ceramics quantified by the Archimedes method. $\rho = \rho_0 \left(\frac{M}{M-M_1}\right)$ where M and M_1 are the weights of samples in air and fluid, the glass density is ρ and the density of toluene is ρ_0 (0.865 g.cm^{-3}) with error ±0.001 g.cm^{-3}. The molar volume can evaluate as $V_m = \frac{M}{\rho}$ where M the molar weight of the glass. Using a pulse-echo method, the ultrasonic velocities estimation was characterized (Echograph model 1085). Besides the density, the velocities were used to evaluate elastic moduli.

longitudinal waves $L = \rho v_l^2$, (1)

transverse waves $G = \rho v_t^2$, (2)

Young's modulus $Y = (1 + \sigma)2G$, (3)

bulk modulus $K = L - \left(\frac{4}{3}\right) G$ (4)

Micro Hardness; $H = \frac{(1-2\sigma)Y}{6(1+\sigma)}$. (5)

3. Results and Discussions

3.1. XRD

The XRD characteristic of B_2O_3-Bi_2O_3-SiO_2- TiO_2 - Y_2O_3 glass with a wide hollow band at 2θ° between (20° - 30°) demonstrated in Fig.1, which signifies the amorphous status of the glass. The width of the small mound differs from one sample to another but is not no indications of the crystalline phases have displayed in all the glasses.

3.2 FT-IR Studies

The vibrations of specific groups of atoms in glass maintained by the vibrations of other atoms. The FT-IR of bismuth titanate borosilicate containing varying amount of Y_2O_3 disclose 3 different bands [20-32]. The band at ~ 680 cm^{-1} assigned to the bending vibrations of the B–O–B linkage in the borate network, the band 800–1200 cm^{-1} to the

stretching of the B–O bonds in BO_4 units, and the bands at 1200–1600 cm^{-1} to the asymmetric stretching relaxation of the B–O bonds in the trigonal BO_3 units. FT-IR spectrum is exemplified in Fig. 2 for these glasses. To get accurate band positions in the FT-IR spectrum, a deconvoluted process signifies used. Residue results obtained plotted to get the quality in the FT-IR deconvolution fitting, and the variation is less than 0.02% in the experimental and simulated graphs. The Gaussian fit of the FT-IR spectrum of these glasses occurs epitomized in Fig. 3 and Table 2. The structural units of the network of these glasses obtained distinguished and summarised as: Band at ~ 445 - 475 cm^{-1} exists related to the vibrations of Si-O-Si and metal cations. Bands in the ~ 487 cm^{-1} exist related to the Bi–O bending vibration from BiO_3 units. Bands at ~ 680 cm^{-1} recognised to (YO_6), (BiO_6), and (TiO_4) vibrations and they overlap with the bending vibrations of the O-Si-O unit. The band at ~ 884 - 894 cm^{-1} is assigned to the to the B–O stretching vibrations in the BO_4 units from diborate groups. The band at ~1035-1065 cm^{-1} remains attributed to stretching vibrations of B–O–Si linkage. Band at ~1110 -1116 cm^{-1} remains assigned to B-O, in BO_4, and a significant component of the asymmetric stretching of the BO_4 tetrahedron. Band at ~ 1235 - 1360 cm^{-1} is assigned to trigonal BO_3 units of B-O bond stretching. Band at ~ 1470 -1496 cm^{-1} assigned to B-O stretching vibrations that principally involve divers' groups of connected oxygen. Band at 1500-1650 cm^{-1} and deformation of H-O-H in glass samples cause B-O symmetric stretching vibrations of various borate groups. Band at 2350, 2853, 2928, and 3415 may be because of the stretching mode of O–H bonds.

To obtain quantitative information about the structural transformations of BO_3 and BO_4 units, the spectra were deconvoluted to their component bands using a Gaussian fit. N_4, fraction of exists characterized by

$$N_4 = \frac{BO4}{(BO4+BO3)} \quad (1)$$

The amount B_4 (mol%), can be characterized as

$$B_4 = N4\ xB2O3 \quad (2)$$

These variations shown in table 2. The results clearly demonstrated that the amount of N_4 and B_4 increases with Y_2O_3 content. The transformation process from BO_3 to BO_4 improves the glasses' consistency. This results in an increase in the coherence of the glass network and the structure stiffening [20-32].

3.3 Structural Studies

Different factors, such as chemical constituents and internal structure have affected the density of $52B_2O_3 - 12SiO_2 - 26Bi_2O_3$-$(10 - x)$ TiO_2- xY_2O_3, $where\ x$: $(0 \leq x \geq 10)$ glass system. Its values are in the range 4.213–5.07 g/cm^3 for different glass compositions and follow a linear trend. The density of the glass under investigation increases with the increment in the content of Y_2O_3. This observation because of the high Y_2O_3 density (5.03 g/cm^3) relative to TiO_2 (4.23 g/cm^3) and the high Y_2O_3 atomic mass (225.81) relative to TiO_2 (79.866). The emergence of Y_2O_3 in a glass matrix enhances the structural network by raising the oxygen level, resulting in the transformation of BO_3 into BO_4 units, and may also another reason lead to an increase in glass density. In the science of glass, the molar volume also plays an important role. The reduction in molar volume could related to the formation of bridging oxygens that reduce the voids within the configuration. The density and molar volume of B_2O_3-Bi_2O_3-SiO_2-TiO_2 - Y_2O_3 glasses exemplified in Fig. 4.

3.4 Thermal studies

We studied the DTA to check the influence of Y_2O_3 on the thermal behaviour of bismuth titanate borosilicate glasses [33]. DTA is a useful technique for indicating modifications due to changes in composition. The glass-transition temperature T_g provides data on both the strength of inter-atomic bonds and the connectivity of the glass network. The stronger $T_g$correlates to a more compact structure, while the less compact structure has a smaller T_g. The DTA curves of prepared glasses are exemplified in Fig. 5. The glass transition

temperature Tg increased with increasing Y_2O_3 according to the DTA graphs from 646 to 663℃. The temperature at which crystallization begins T_c, increased with increasing Y_2O_3, from 732 to 784°C. As shown in Table 4, the end-set of crystallization temperature Tp increased with increasing Y_2O_3, rising from 761 to 813°C. This enhances resulting in significant increase in average force, interconnection, and compression force. Thermal stability, and weighted thermal stability projected by

$$\Delta T = T_c - T_g \quad (3)$$

$$H_g = \frac{\Delta T}{T_g} \quad (4)$$

$$\mathrm{S} = (T_p - T_c)\frac{\Delta T}{T_g} \quad (5)$$

From Table 4, It exists perceived that the thermal stability increases from 86 to 121 ℃ with the increase in Y_2O_3 content. The increase Y_2O_3 at expense of TiO_2 increases the formation of BO, the stronger Y–O–B bonds establishment. Hence, such type of behavior depicts the existence of BO and the development of bridging oxygen with substitution of Y_2O_3 that followed depolymerization of a glassy network.

3.5 XRD and SEM studies

As shown in Fig. 6, the glass-ceramics obtained investigated further using XRD. The XRD curves of G1, G3, and G5 are comparable, with the exception that the diffraction peaks are stronger. Y_2O_3 could break the network of bismuth borosilicate units and behave as a stabilizing agent, enhancing chemical structure and mechanical rigidity. Lanthanum titanium silicate is the most powerful phase, $La_2(Ti_2SiO_9)$, card No. 01-082-1490, Lanthanum titanium silicate oxide has a lower phase $La_4Ti_5\ (Si_2O_7)_2O_8$ card No. 01-083-023, and lead borosilicate ($PbSiBO_7$) card No. 01- 13-0484. The increase in Y_2O_3 (Trimounsite-(Y)) $Y_2Ti_2SiO_9$ card No. 00-046-1375 has resulted in the formation of new phases.

SEM used to check the microstructure of glass-ceramics, as shown in Figs. 7&8. It does confirm that the glass composition has uniform distributions. Fig. 7 depicts the micrograph (G1). On the surface, it appears to be nearly unchanged. Lanthanum Titanium Silicate formed in a random crystalline texture with larger interstitial pores that represent the residual glassy matrix. Fig. 8 depict the micrographic of (G5). It does suggest that the glass composition has uniform distributions. The possibility of crystallization enhances as the Y_2O_3 concentration raised.

3.6 Mechanical studies

Figure 9 exemplified density and micro-hardness of a glass-ceramics increasing trend as the Y_2O_3 content increases. Figure 9 exemplified the ultrasonic velocities glass-ceramic samples. As exemplified in Fig. 10, the ultrasonic velocity of these samples enhanced by an increment in the Y_2O_3 concentration. Particularly, the increment in ultrasonic velocities was due to an increment in the network structure's connectivity, and to increase in the internal energy.

In this article, the elastic-moduli of glass-ceramics were calculated and are shown in Fig. 11 and Table 5. It does show that the addition of Y_2O_3 content resulted in a significant increase in elastic moduli values.

4. Conclusions

The influence of varying Fe_2O_3 content on the structure of glasses and glass-ceramics properties of iron aluminoleadborate glasses with the form $55B_2O_3$ - $30Pb_3O_4$ - $(15 - x)Al_2O_3$ - xFe_2O_3, $where\ x = 0, 1, 2, 4, and\ 5$ mol % have illustrated in this investigation. XRD measurements evaluated the amorphous nature of the glasses. Molar volume obtained reduced while the density denotes increased in the present system. With an increase in yttrium concentration, the FT-IR spectral shifts to higher wavenumbers. Also, the structure becomes more compact by incorporating Y_2O_3, as YO_6 species produced. Boron transforms from BO_3

into BO_4 tetrahedra after iron incorporated. This results in an increase in the coherence of the glass network and the structure stiffening. As the Y_2O_3 content in these glasses increased, so their thermal stability increase. These increases associated with the increase in the glass structure's connection. The glass-ceramic signified manufactured and investigated using XRD, SEM, and mechanical properties. XRD outcomes informed all the expected phases because of the crystallization process. The glass composition was found to be distributed in SEM images of selected glass-ceramic samples.

Author contributions: Kh. S. Shaaban: performing, XRD, mechanical measurements and analysis, Writing-review, writing the manuscript, Methodology, Software, and writing – discussion.

Acknowledgments:

Availability of data and material: My manuscript and associated personal data will be shared with Research Square for the delivery of the author dashboard.

Compliance with ethical standards: The manuscript has not been published elsewhere and has not been submitted simultaneously for publication elsewhere.

Conflict of interest: The authors declare that they have no conflict of interest.

Declaration of Competing Interest: The authors declare that they have no known competing financial interests or personal relationships that could have appeared to influence the work reported in this paper.

Funding statement: There are currently no Funding Sources on the list

Consent to participate: The authors consent to participate.

Consent for Publication: The author's consent for publication.

References

[1] Shaaban, K. S., Abo-Naf, S. M., & Hassouna, M. E. M. Physical and Structural Properties of Lithium Borate Glasses Containing MoO_3. Silicon **11,** 2421–2428, (2019). DOI:10.1007/s12633-016-9519-4

[2] El-Rehim, A.F.A., Shaaban, K.S. (2021), Influence of La_2O_3 content on the structural, mechanical, and radiation-shielding properties of sodium fluoro lead barium borate glasses. J Mater Sci: Mater Electron. https://doi.org/10.1007/s10854-020-05204-7

[3] Shaaban, K. S., Abo-naf S. M., Abd Elnaeim, A. M., & Hassouna, M. E. M. Studying effect of MoO_3 on elastic and crystallization behavior of lithium diborate glasses. Applied Physics A, 123(6) 457, (2017). DOI:10.1007/s00339-017-1052-9

[4] Rao, L. S., Reddy, M. S., Rao, D. K., & Veeraiah, N. Influence of redox behavior of copper ions on dielectric and spectroscopic properties of Li_2O–MoO_3–B_2O_3: CuO glass system. Solid-State Sciences, 11(2), 578–587. (2009). DOI: 10.1016/j.solidstatesciences.2008.06.022

[5] Abd-Allah, W.M., Saudi, H.A., Shaaban, K.S. *et al.* Investigation of structural and radiation shielding properties of $40B_2O_3$–30PbO–(30-*x*) BaO-*x* ZnO glass system. Appl. Phys. A **125,** 275 (2019). https://doi.org/10.1007/s00339-019-2574-0

[6] Saudi, H.A., Abd-Allah, W.M. & Shaaban, K.S. Investigation of gamma and neutron shielding parameters for borosilicate glasses doped europium oxide for the immobilization of radioactive waste. J Mater Sci: Mater Electron **31,** 6963–6976 (2020). https://doi.org/10.1007/s10854-020-03261-6

[7] Somaily, H.H., Shaaban, K.S., Makhlouf, S.A. *et al.* Comparative Studies on Polarizability, Optical Basicity and Optical Properties of Lead Borosilicate Modified with Titania. J Inorg Organomet Polym (2020). https://doi.org/10.1007/s10904-020-01650-2

[8] Wahab, E. A. A., & Shaaban, K. S. Effects of SnO_2 on spectroscopic properties of borosilicate glasses before and after plasma treatment and its mechanical properties. Materials Research Express, 5(2), 025207, (2018). https://doi.org/10.1088/2053-1591/aaaee8

[9] Koubisy, M.S.I., Shaaban, K.S., Wahab, E.A.A. *et al.* (2021), Synthesis, structure, mechanical and radiation shielding features of $50SiO_2$–$(48+X)$ $Na_2B_4O_7$–$(2-X)$ MnO_2 glasses. Eur. Phys. J. Plus **136,** 156, https://doi.org/10.1140/epjp/s13360-021-01125-4

[10] E.A. Abdel Wahab, M.S.I. Koubisy, M.I. Sayyed, K.A. Mahmoud, A.F. Zatsepin, Sayed A. Makhlouf, Shaaban, Kh.S. (2021), Novel borosilicate glass system: $Na_2B_4O_7$-SiO_2-MnO_2 Synthesis, average electronics polarizability, optical basicity, and gamma-ray shielding features, Journal of Non-Crystalline Solids, 553,120509, doi.org/10.1016/j.jnoncrysol.2020.120509

[11] El-Rehim, A.F.A., Zahran, H.Y., Yahia, I.S. *et al.* (2020). Physical, Radiation Shielding and Crystallization Properties of Na_2O-Bi_2O_3- MoO_3-B_2O_3- SiO_2 Fe_2O_3 Glasses. Silicon, doi.org/10.1007/s12633-020-00827-1

[12] Shaaban, K.S., Yousef, E.S., Abdel Wahab, E.A. *et al.* (2020). Investigation of Crystallization and Mechanical Characteristics of Glass and Glass-Ceramic with the Compositions xFe_2O_3-$35SiO_2$-$35B_2O_3$-$10Al_2O_3$-$(20-x)$ Na_2O. J. of Materi Eng and Perform. https://doi.org/10.1007/s11665-020-04969-6

[13] El-Rehim, A.F.A., Zahran, H.Y., Yahia, I.S. *et al.* Structural, Elastic Moduli, and Radiation Shielding of SiO_2-TiO_2-La_2O_3-Na_2O Glasses Containing Y_2O_3. J. of Materi Eng and Perform (2021). https://doi.org/10.1007/s11665-021-05513-w

[14] El-Sharkawy, R. M., Shaaban, K. S., Elsaman, R., Allam, E. A., El-Taher, A., & Mahmoud, M. E. (2020). Investigation of mechanical and radiation shielding characteristics of novel glass systems with the composition xNiO-20ZnO-$60B_2O_3$-(20-x) CdO based on nano metal oxides. Journal of Non-Crystalline Solids, 528,119754 doi: 10.1016/j.jnoncrysol.2019.119754

[15] Shaaban, K.S., Zahran, H.Y., Yahia, I.S. et al. (2020), Mechanical and radiation-shielding properties of B_2O_3–P_2O_5–Li_2O–MoO_3 glasses. Appl. Phys. A 126, (10), 804. https://doi.org/10.1007/s00339-020-03982-9

[16] Shaaban, K.S., Koubisy, M.S.I., Zahran, H.Y. et al. (2020). Spectroscopic Properties, Electronic Polarizability, and Optical Basicity of Titanium–Cadmium Tellurite Glasses Doped with Different Amounts of Lanthanum. J Inorg Organomet Polym. https://doi.org/10.1007/s10904-020-01640-4

[17] El-Rehim, A.A., Zahran, H., Yahia, I. *et al.* (2020). Radiation, Crystallization, and Physical Properties of Cadmium Borate Glasses. Silicon https://doi.org/10.1007/s12633-020-00798-3

[18] Shaaban, K.S., Yousef, E.S., Mahmoud, S.A. *et al.* (2020). Mechanical, Structural and Crystallization Properties in Titanate Doped Phosphate Glasses. J Inorg Organomet. Polym https://doi.org/10.1007/s10904-020-01574-x

[19] Şakar, E., Özpolat, Öü.Fı., Alım, Bü., Sayyed, M.I., Kurudirek, M., (2020). PhyX / PSD: Development of a user friendly online software for calculation of parameters relevant to radiation shielding and dosimetry, Radiation Physics and Chemistry 166, 108496, https://doi.org/10.1016/j.radphyschem.2019.108496

[20] Rejisha, S. R., Anjana, P. S., & Gopakumar, N. (2016), Effect of cerium (IV) oxide on the optical and dielectric properties of strontium bismuth borate glasses. J Mater Sci: Mater Electron, 27(5), 5475- 5482, DOI 10.1007/s10854-016-4452-2

[21] Gautam, C., Yadav, A. K., & Singh, A. K. (2012). A Review on Infrared Spectroscopy of Borate Glasses with Effects of Different Additives. ISRN Ceramics, 2012, 1 -17. doi:10.5402/2012/428497

[22] R. V. Adams and R. W. Douglas, (1959) Infra-red studies on various samples of fused silica with special reference to the bands due to water, Journal of The Society of Glass Technology,.43, 147–158.

[23] H. Scholzelt, Glass: Nature, Structure and Properties, Springer, New York, NY, USA, 1991

[24] J. Krogh-Moe, (1965). Interpretation of the infra-red spectra of boron oxide and alkali borate glasses," Physics and Chemistry of Glasses, 6, 46–54.

[25] A. Varshneya, Fundamentals of Inorganic Glasses, Academic Press, New York, NY, USA, 1994.

[26] A. S. Tenny and J. Wong, (1972), Vibrational spectra of vapor deposited binary borosilicate glasses, Journal of Chemical Physics, 56, 5516–5523.

[27] Morsi, R. M. M., Basha, M. A. F., & Morsi, M. M. (2016). Synthesis and physical characterization of amorphous silicates in the system SiO_2-Na_2O– RO (R=Zn, Pb or Cd). Journal of Non-Crystalline Solids, 439, 57–66. doi: 10.1016/j.jnoncrysol.2016.02.018

[28] El-Rehim, A.F.A., Zahran, H.Y., Yahia, I.S. *et al.* (2020). Physical, Radiation Shielding and Crystallization Properties of Na_2O-Bi_2O_3- MoO_3-B_2O_3- SiO_2-Fe_2O_3 Glasses. Silicon https://doi.org/10.1007/s12633-020-00827-1

[29] Koubisy, M.S.I., Shaaban, K.S., Wahab, E.A.A. *et al.* (2021), Synthesis, structure, mechanical and radiation shielding features of $50SiO_2$–$(48 + X)$ $Na_2B_4O_7$–$(2 - X)$ MnO_2 glasses. Eur. Phys. J. Plus **136,** 156, https://doi.org/10.1140/epjp/s13360-021-01125-4

[30] El-Rehim, A.F.A., Shaaban, K.S. Influence of La_2O_3 content on the structural, mechanical, and radiation-shielding properties of sodium fluoro lead barium borate glasses. *J Mater Sci: Mater Electron* **32,** 4651–4671 (2021). https://doi.org/10.1007/s10854-020-05204-7

[31] Shaaban, K.S., Wahab, E.A.A., Shaaban, E.R. et al. (2020). Electronic polarizability, optical basicity and mechanical properties of aluminum lead phosphate glasses. Opt Quant Electron **52,** 125 https://doi.org/10.1007/s11082-020-2191-3

[32] Shaaban, K.S., Wahab, E.A.A., Shaaban, E.R. et al. (2020). Electronic Polarizability, Optical Basicity, Thermal, Mechanical and Optical Investigations of $(65B_2O_3$–$30Li_2O$–$5Al_2O_3)$ Glasses Doped with Titanate. Journal of Elec Materi 49, 2040–2049. https://doi.org/10.1007/s11664-019-07889-x

[33] S. Singh, G. Kalia and K. Singh, (2015), Effect of Intermediate Oxide (Y_2O_3) on Thermal, Structural and Optical Properties of Lithium Borosilicate Glasses, Mol. Struct., **1086**, 239–245. https://doi.org/10.1016/j.molstruc.2015.01.031

Figures

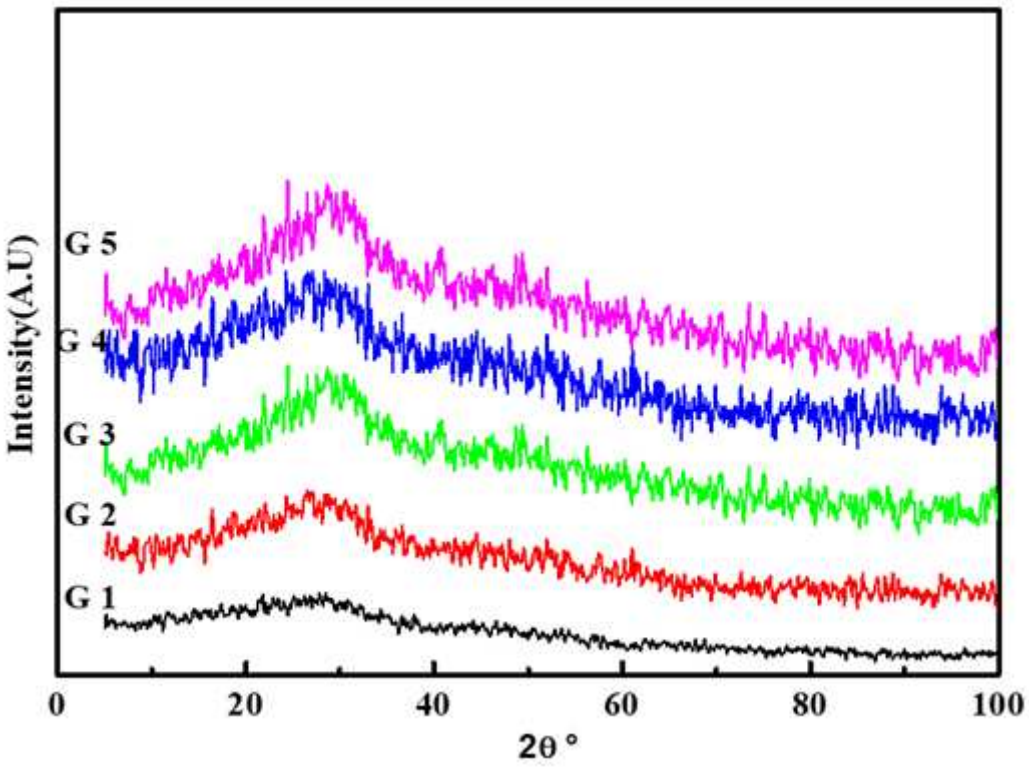

Figure 1

XRD of the studied glasses.

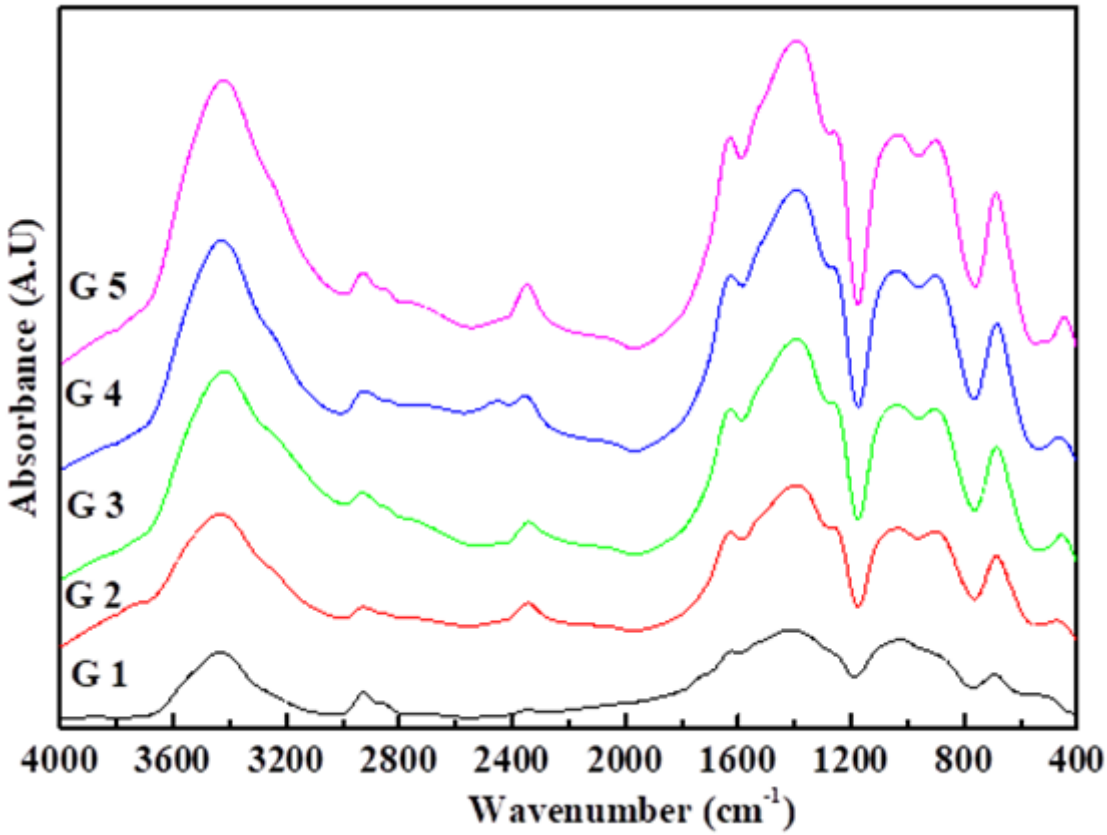

Figure 2

Infrared spectra of the investigated bismuth titanate borosilicate glasses doped Y2O3.

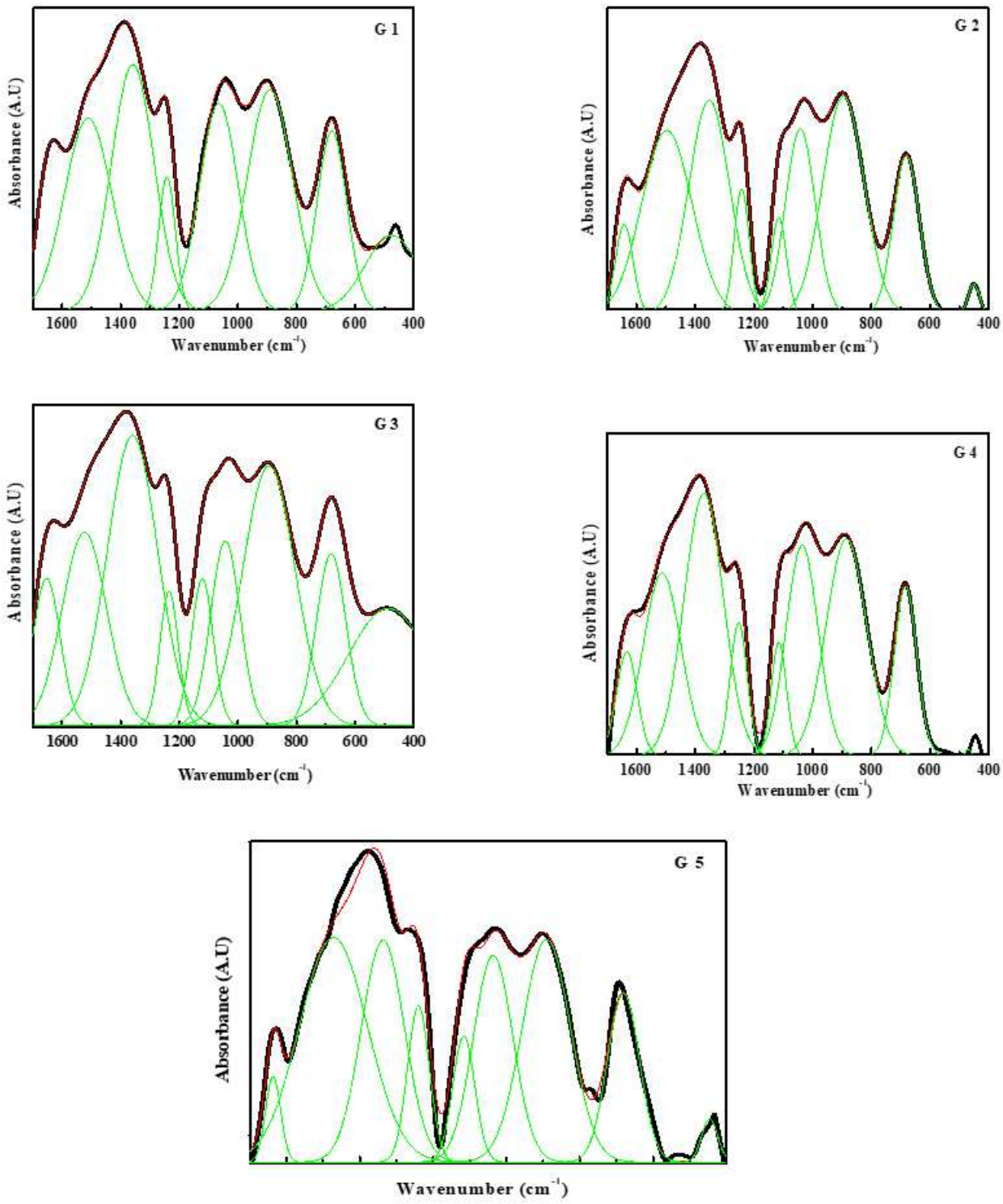

Figure 3

Curve-fitting of IR spectra of the investigated bismuth titanate borosilicate glasses doped Y2O3.

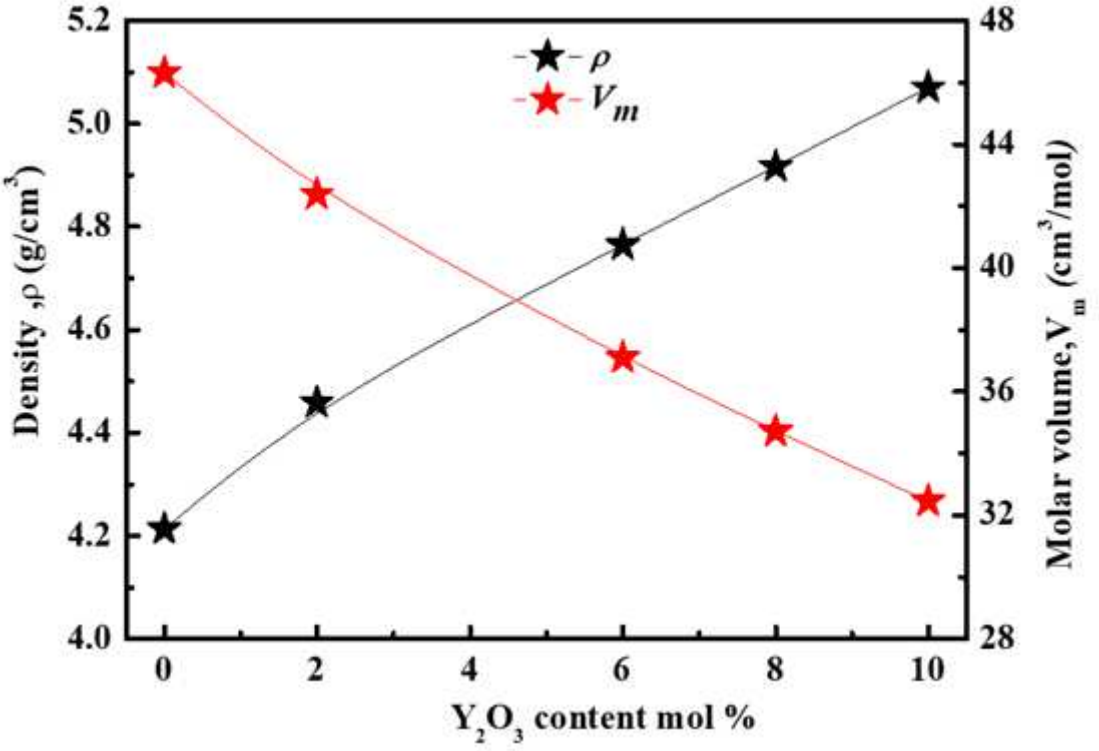

Figure 4

Density and molar volume of the prepared samples versus Y2O3 concentration in mol %.

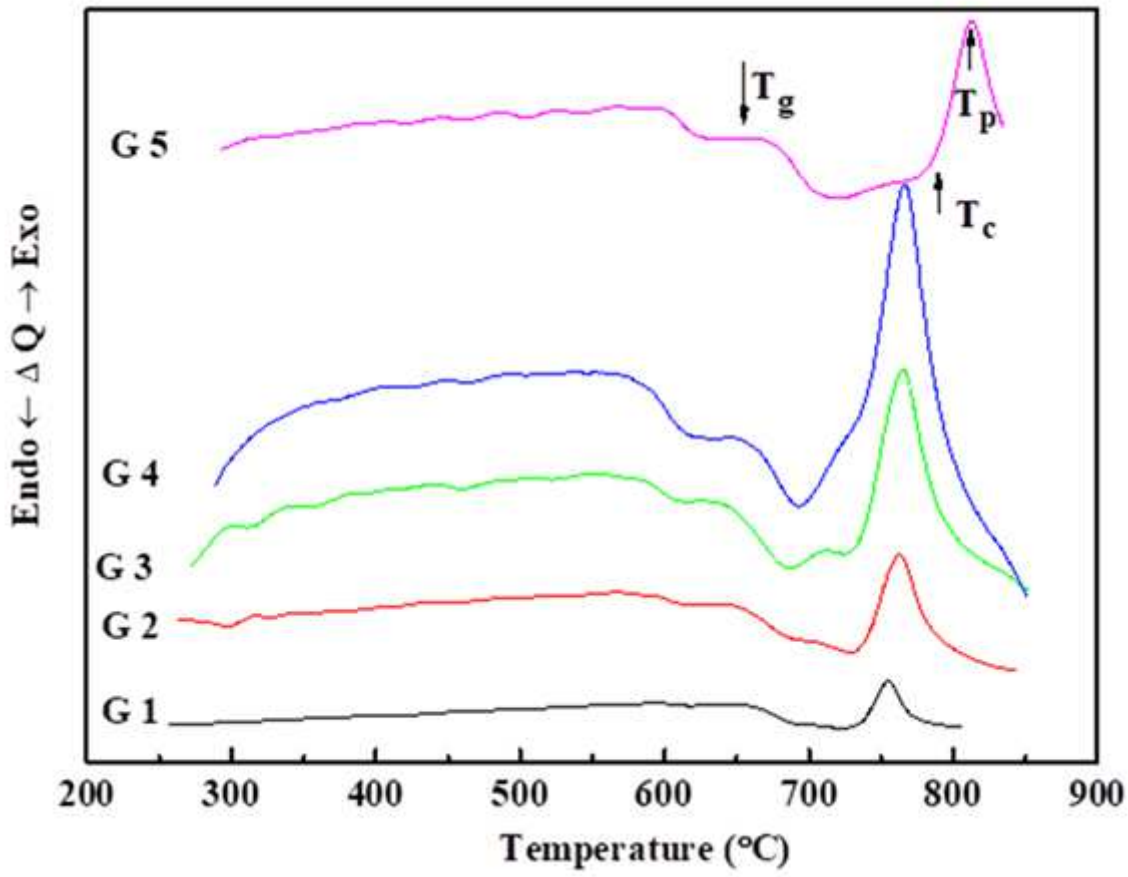

Figure 5

DTA of the of the investigated bismuth titanate borosilicate glasses doped Y2O3.

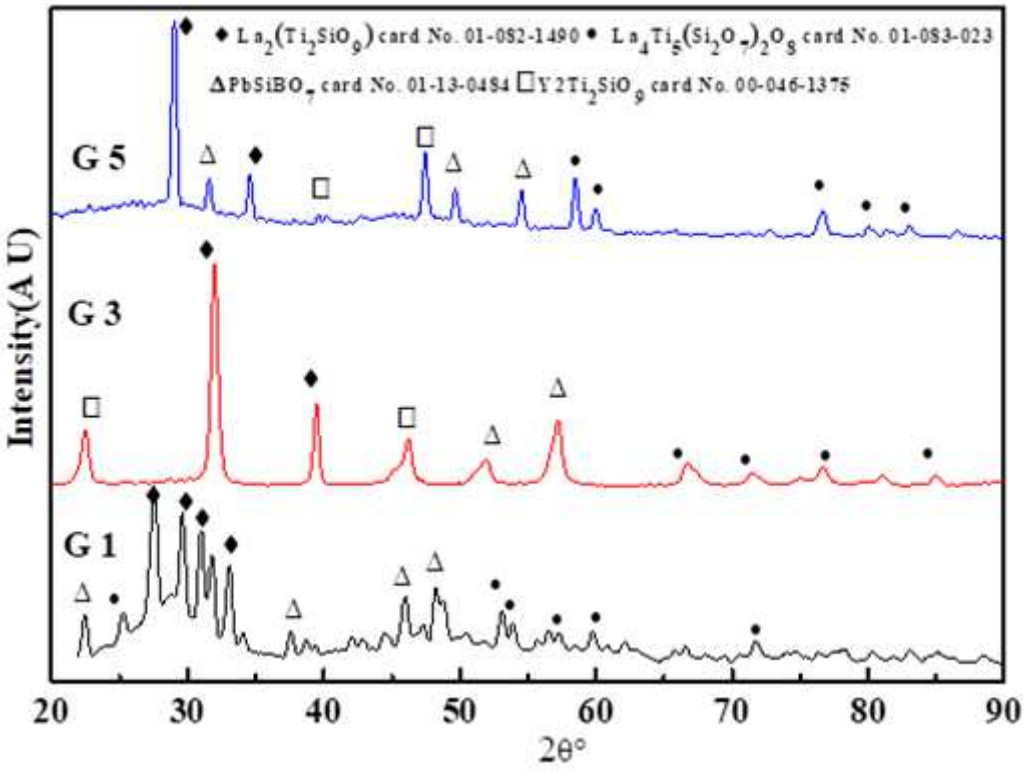

Figure 6

The XRD of the selected glass-ceramics.

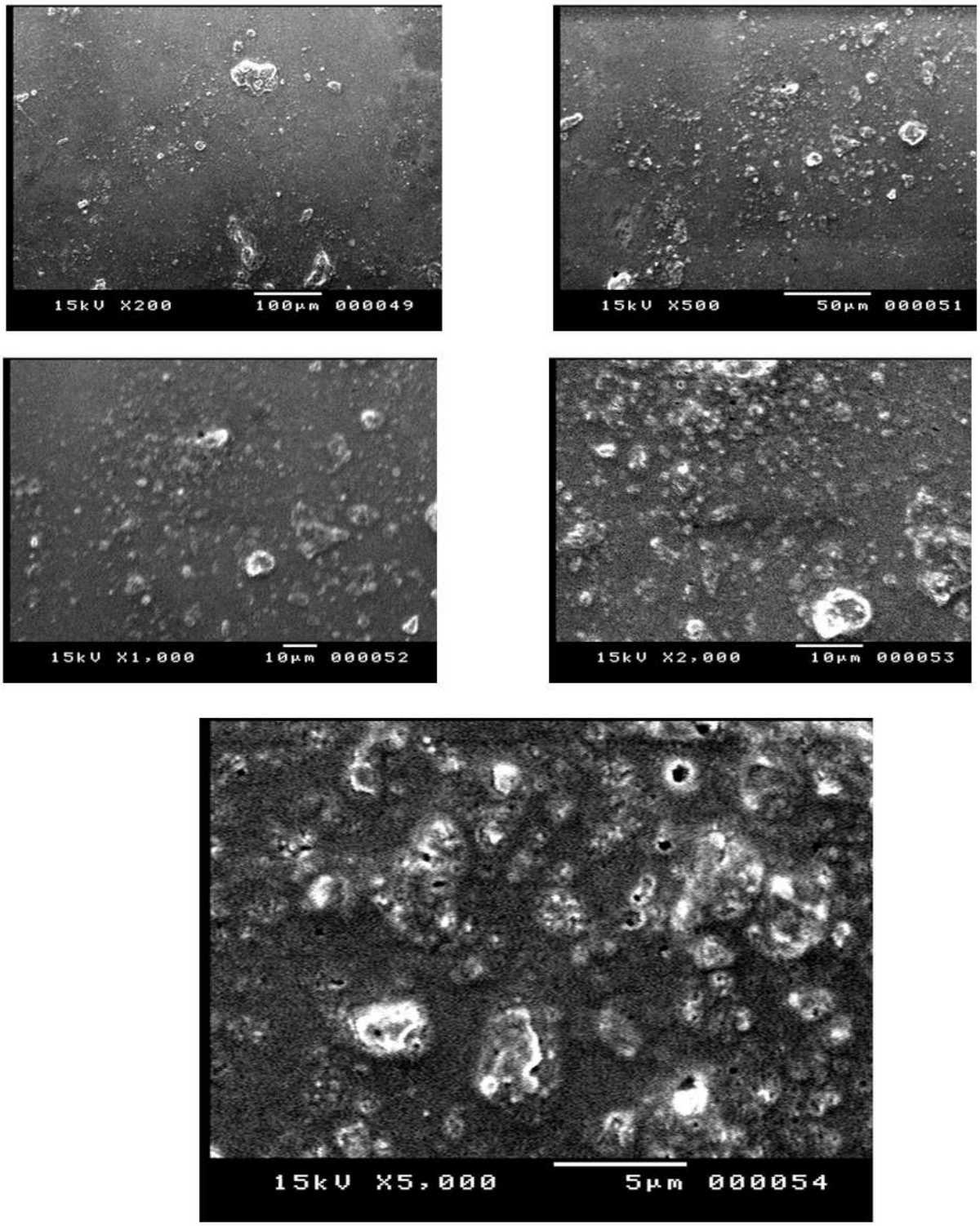

Figure 7

SEM backscattered electron images of the produced glass-ceramics (G 1)

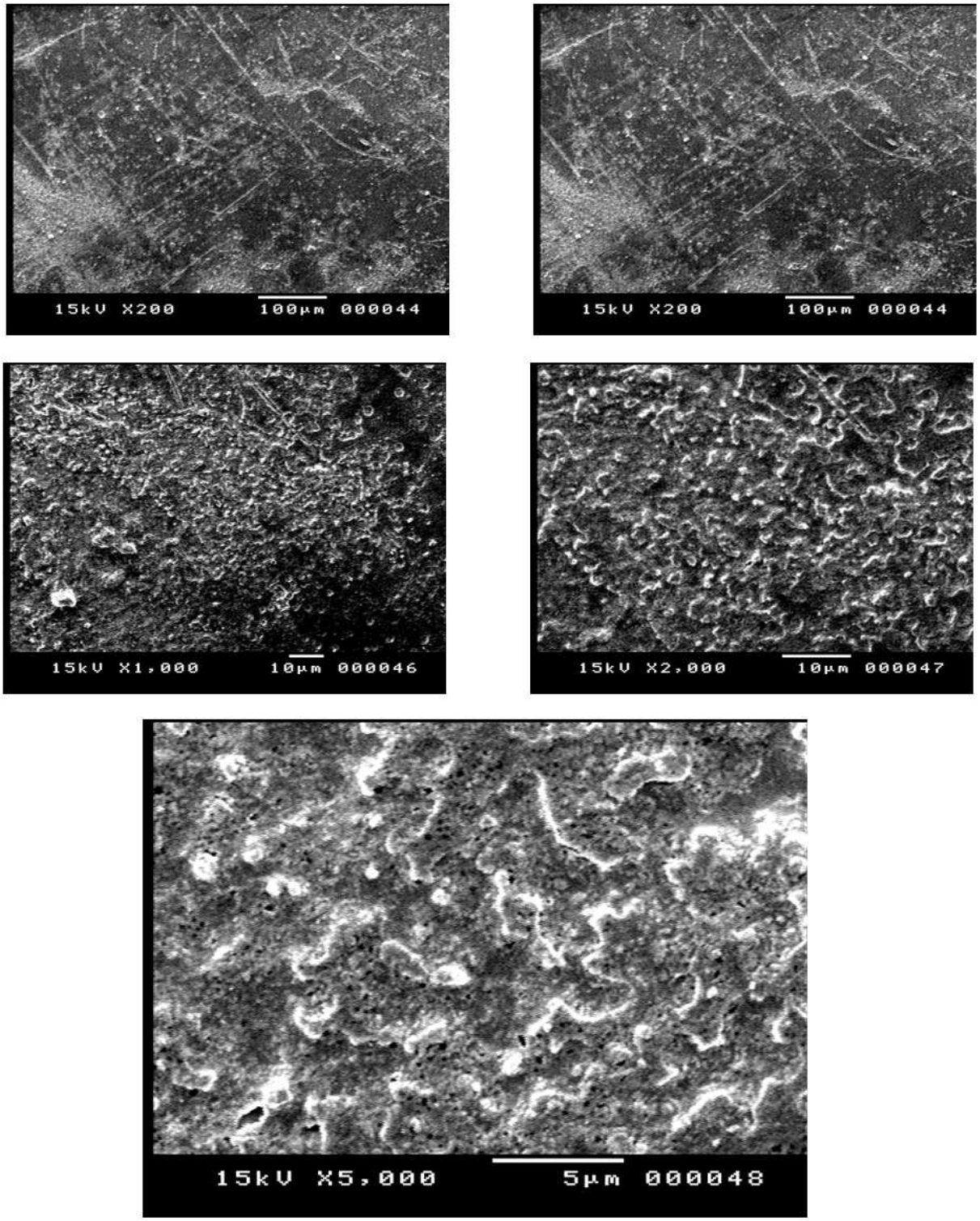

Figure 8

SEM backscattered electron images of the produced glass ceramics (G 5)

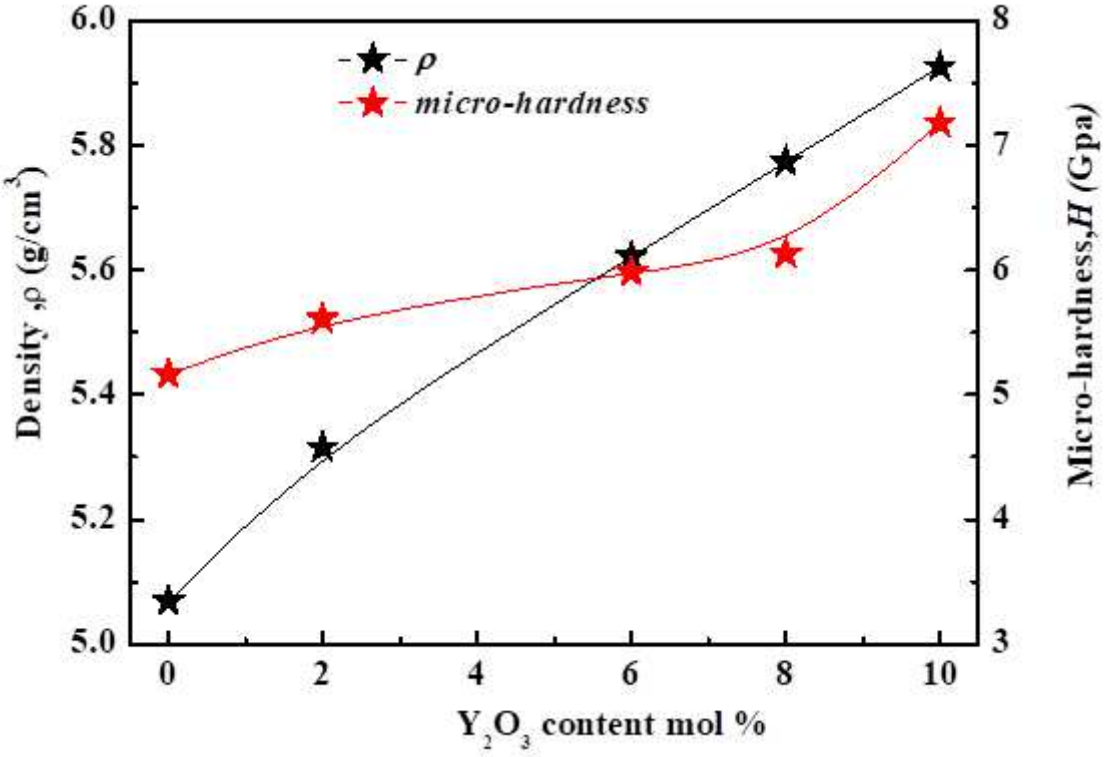

Figure 9

Density and micro-hardness of the prepared samples versus Y2O3 concentration in mol %.

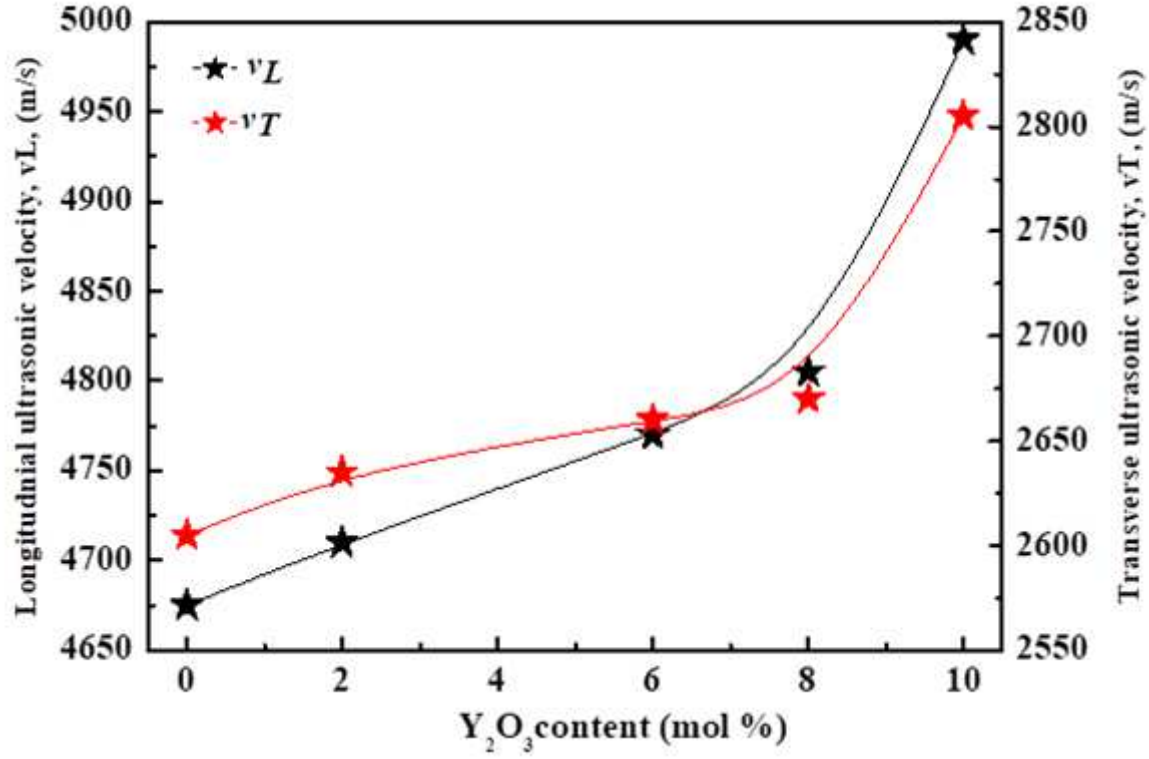

Figure 10

Dependence of the longitudinal and shear ultrasonic velocities vL and vT of the investigated glass-ceramics with Y2O3 concentration by mol. %.

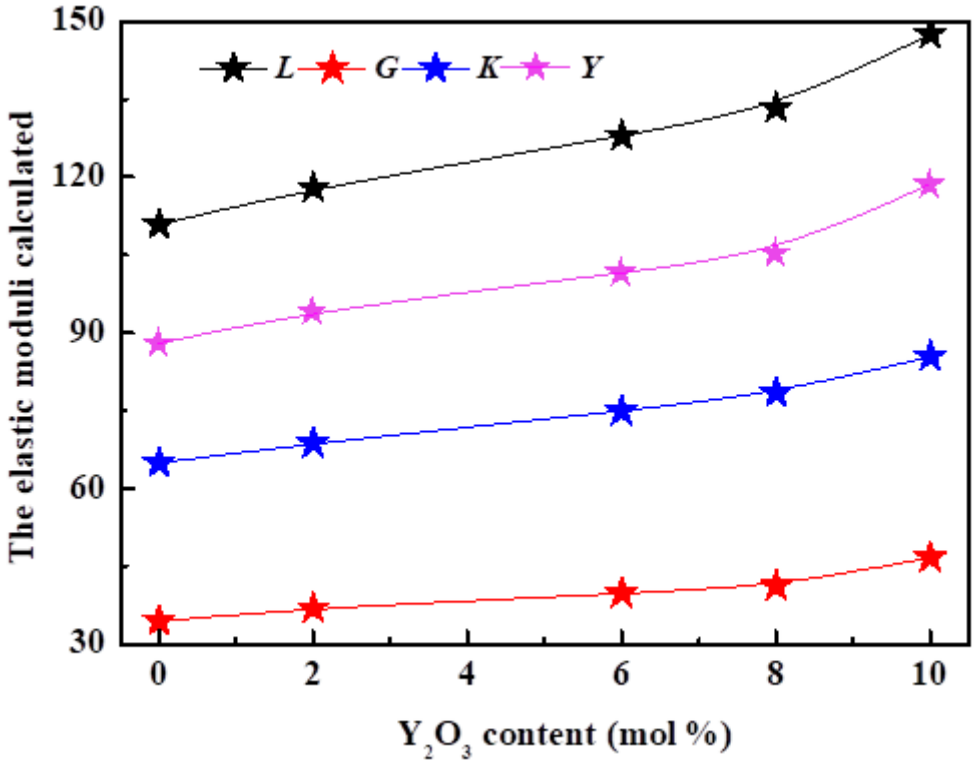

Figure 11

Elastic moduli of the studied glass-ceramics with Y2O3 content by mol. %.